

Dynamicals of a Limit Cycle Oscillator under Time Delayed Linear and Nonlinear Feedbacks

D. V. Ramana Reddy^y, A. Sen^z, and G. L. Johnston
 Institute for Plasma Research, Bhat, Gandhinagar 382 428
 (February 5, 2020)

We study the effects of time delayed linear and nonlinear feedbacks on the dynamics of a single Hopf bifurcation oscillator. Our numerical and analytic investigations reveal a host of complex temporal phenomena such as phase slips, frequency suppression, multiple periodic states and chaos. Such phenomena are frequently observed in the collective behavior of a large number of coupled limit cycle oscillators. Our time delayed feedback model offers a simple paradigm for obtaining and investigating these temporal states in a single oscillator. We construct a detailed bifurcation diagram of the oscillator as a function of the time delay parameter and the driving strengths of the feedback terms. We find some new states in the presence of the quadratic nonlinear feedback term with interesting characteristics like phase reversals, radial trapping, spiraling patterns in the amplitude space, and biorhythmicity. Our results may find useful applications in physical, chemical or biological systems.

PACS numbers : 05.45.+b, 87.10.+e

Keywords: Limit cycle oscillator; Time delay; Feedback; Phase Slips; Spiraling solution; Biorhythmicity

I. INTRODUCTION

Coupled limit cycle oscillators have been extensively studied in recent times as a mathematical model for understanding the collective behavior of a wide variety of physical, chemical and biological problems [1{12]. One of the simplest and earliest of such models is the so called Kuramoto model [5], which is a mean field model of a collection of phase oscillators and clearly exhibits such cooperative phenomena as spontaneous synchronization of the oscillators beyond a certain coupling strength. A more generalized version of the Kuramoto model that includes both phase and amplitude variations, exhibits collective behavior like amplitude death, where for a large enough spread in the natural frequencies of the oscillators, an increase in the coupling strength induces a stabilization of the origin, leading to a total cessation of oscillations in the system [13{16]. Other collective states observed in these models include partial synchronization, phase trapping, large amplitude Hopf oscillations and even chaotic behavior [15,16]. Recently there has been some interest in investigating the effect of time delay on the collective dynamics of these coupled models [17{24]. Time delay is ubiquitous in most physical [25,26], chemical [27], biological [28], neural [29], ecological [30], and other natural systems due to finite propagation speeds of signals, finite processing times in synapses, finite reaction times, etc. Time delayed coupling introduces interesting new features in the collective dynamics e.g. simultaneous existence of several different synchronized states [17{20],

regions of amplitude death even among identical oscillators [21,22], bistability between synchronized and incoherent states [20,23], etc.

One of the remarkable aspects of this cooperative dynamics is that many of its salient features can be observed even in a system consisting of just two coupled oscillators [14,17,21,22]. The temporal behavior of either of the two oscillators in such a case (which is easy to investigate both numerically and analytically) reveals a great deal about the collective aspects of larger systems. In fact, a useful point of view to adopt is to regard each oscillator as being driven autonomously by a source term that represents the collective feedback of the rest of the system. Motivated by such a qualitative consideration, we have studied in detail the dynamics of the following model system of an autonomously driven single limit cycle oscillator,

$$Z(t) - (a + i\omega_0)Z(t) + jZ(t)^2)Z(t) = f(Z(t)), \quad (1)$$

where $Z(t) = X + iY$ is a complex quantity, ω_0 is the frequency of oscillation, a is a real constant and τ is the time delay of the autonomous feedback term f . The latter is modelled as,

$$f(Z(t)) = K_1 Z(t) - K_2 Z^2(t); \quad (2)$$

where K_1 and K_2 represent the strengths of the linear and nonlinear contributions of the feedback. The fundamental oscillator of our model (the left-hand side of Eq. (1)) is the basic unit of the generalized Kuramoto

Present address: 12 Billings St., Acton, MA 01720, USA.

model and has a stable limit cycle of amplitude \bar{a} with angular frequency ω . It is simply the normal form of a supercritical Hopf bifurcation and is a useful nonlinear model for a variety of physical, chemical and biological systems.

Eq. (1) can therefore be also viewed as a prototype equation arising in the delayed feedback control of an individual physical or biological entity that can be modelled by the normal form. Our results may thus be of more general and direct utility in addition to providing useful insights into the collective dynamics of large systems. Similar studies (using a variety of feedback terms) exist for the damped harmonic oscillator for example [31], but we are not aware of such investigations for our model limit cycle oscillator. A few investigations in the past have restricted themselves to the study of noise and perturbations [32-34] on the dynamics of such an oscillator.

The organization of our paper is as follows. In Section II, we analyse the dynamics of the oscillator using just the linear feedback term and discuss the analytic conditions for the stability of the origin and the existence of periodic orbits. Detailed bifurcation diagrams are plotted as a function of the various system parameters like a , K and τ and their similarity to collective states of larger systems is pointed out. We also present numerical results on higher frequency states, which can coexist with the lowest periodic state and discuss the phenomenon of frequency suppression of these states as a function of the time delay parameter. Section III treats the full feedback term by including the quadratic nonlinear contribution. The bifurcation diagram is a great deal richer now due to the existence of two other equilibrium points in addition to the origin. We analyse the stability of these equilibria and the consequent temporal behavior of the oscillator in various parameter regimes. Some novel temporal states are pointed out. Section IV summarizes our results and discusses their significance and possible applications.

II. TIME DELAYED LINEAR FEEDBACK

We begin our analysis of the model Eq. (1) by considering only the linear feedback term (i.e. $K_2 = 0$), so that we have,

$$\dot{Z}(t) = (a + i\omega - jZ(t))Z(t) - KZ(t); \quad (3)$$

where we have put $K_1 = K$ for simplicity of notation. Note that the above linear feedback term is similar in form to the feedback term used extensively in experimental and theoretical investigations of control of chaos using the Pyragas method [35]. The actual form in the Pyragas method is $(Z(t) - Z(t))$, which is equivalent to replacing the constant a by $a + K$ in the above equation. However, unlike the systems investigated for the Pyragas method, Eq. (3) has no regimes of chaotic behavior. We will examine instead the effect of the time

delayed feedback on the stability of the origin and on the nature of the periodic solutions.

In the absence of time delay, it is clear from inspection that Eq. (3) has a time asymptotic periodic solution given by $Z(t) = \bar{a} \frac{P}{K} e^{i\omega t}$ for $a > K$. If $a < K$, then the origin is the only stable solution; or, in other words, no oscillatory time-asymptotic solutions are possible. We now carry out a more systematic study of the stability of the origin in the presence of time delay.

A. Stability of the origin

The origin $Z_p = (0; 0)$ is a fixed point of Eq. (3). To study its stability we assume that the perturbations about Z_p grow as $e^{\lambda t}$, where λ is a complex number. Substituting in Eq. (3) and linearizing about $Z = Z_p$, one easily obtains the following characteristic equation:

$$\lambda = a - i\omega - K e^{i\omega t}; \quad (4)$$

where the i sign arises from considering the complex conjugate of Eq. (3). This ensures that we have the complete set of eigenvalues. For $\omega = 0$, one obtains $\lambda = a - K$. The origin is stable in the region of parameter space where $\text{Re}(\lambda) < 0$, which occurs when $K > a$. So the critical, or the marginal stability, curve is given in this case by $K = a$. When $\omega \neq 0$, Eq. (4) remains a transcendental equation with a principal term ω and hence the equation possesses an infinite number of complex solutions. Let these roots be ordered according to the magnitude of the real parts: $\lambda_1, \lambda_2, \dots, \lambda_n$, where $\text{Re}(\lambda_1) < \text{Re}(\lambda_2)$. The problem of finding the stability criterion then reduces to that of finding the conditions on K and ω such that $\text{Re}(\lambda_j) < 0$, for all j . Let $\lambda = \mu + i\nu$, where μ and ν are real. Substituting this in Eq. (4) we get:

$$\mu = a - K \cos(\omega t); \quad (5)$$

$$\nu = \omega + K \sin(\omega t); \quad (6)$$

We can arrive at the following two equations for μ and ν by squaring and adding the above two equations and by dividing the first equation by the second respectively:

$$\mu = \omega + \frac{P}{K^2 e^{2\omega t}} (a - \mu)^2; \quad (7)$$

$$\nu = a - (\omega + \mu) = \tan(\omega t); \quad (8)$$

where, in the above and from here after, we consider only one set of curves by choosing $\omega = +\sqrt{\frac{P}{K^2}}$. The other set of curves arising due to $\omega = -\sqrt{\frac{P}{K^2}}$ is implicit in the above since the eigenvalues always occur in complex conjugate pairs. From Eq. (7) we see that μ is real only when $(a - \mu)^2 e^{2\omega t} < K^2$. So for any finite value of K , the value of μ is bounded from above. To obtain the critical curves, set $\mu = 0$. This gives

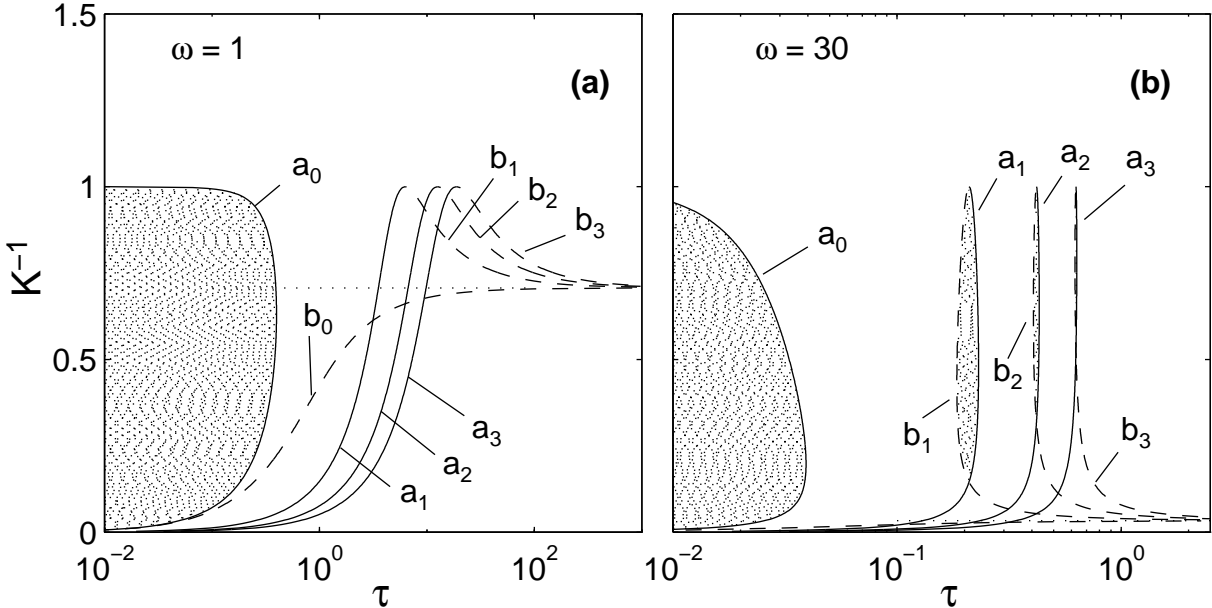


FIG. 1. The stability of the origin is shown in a (τ, K^{-1}) diagram for (a) $\omega = 1$, $a = 1$ and (b) $\omega = 30$, $a = 1$. At lower values of ω there is only one death region that is confined between $\tau = 0$ and $\tau = \tau_1(0; K)$, but for higher values of ω there are generally multiply connected regions of amplitude death. The curves a_n and b_n represent $\tau_1(n; K)$ and $\tau_2(n; K)$ respectively. The dotted horizontal line is $\tau = f(\omega)$.

$$j_{=0} = \omega \frac{p}{K^2 - a^2}; \quad (9)$$

and by inverting Eq. (5) and choosing the correct signs, we obtain the following two sets of critical curves:

$$\tau_1(n; K) = \frac{2n + \cos^{-1}(a=K)}{\omega + \frac{p}{K^2 - a^2}}; \quad (10)$$

$$\tau_2(n; K) = \frac{2n - \cos^{-1}(a=K)}{\omega - \frac{p}{K^2 - a^2}}; \quad (11)$$

$n = 1, 2, \dots$: Thus the critical curves exist only in the region $K > a$. Since for $\tau = 0$, the region of stability of the origin is given by $K > a$, the corresponding region for $\tau > 0$, will be given by the area between $\tau = 0$ and the critical curve closest to the line $\tau = 0$. This critical curve should be the one on which $d = d > 0$. From Eq. (4),

$$\frac{d}{d\tau} = \frac{K e}{1 - K e}; \quad (12)$$

and

$$\begin{aligned} \frac{d}{d\tau} j_{=0} &= \operatorname{Re} \frac{K(i)e^{i\tau}}{1 - K e^{i\tau}} \\ &= K \sin(\tau) D^{-1} = (\omega - !) D^{-1}; \end{aligned} \quad (13)$$

where $D = [1 - K \cos(\tau)]^2 + [K \sin(\tau)]^2$ is real and positive. Hence,

$$\begin{aligned} \frac{d}{d\tau} j_{=0} &\stackrel{8}{\gtrless} 0 \text{ on } \tau_1, \\ &\stackrel{8}{\gtrless} 0 \text{ on } \tau_2 \text{ if } K > f(\omega), \\ &\stackrel{8}{=} 0 \text{ on } \tau_2 \text{ if } K = f(\omega), \\ &\stackrel{8}{\lessdot} 0 \text{ on } \tau_2 \text{ if } K < f(\omega), \end{aligned} \quad (14)$$

where $f(\omega) = \frac{p}{a^2 + \omega^2}$. The above condition implies that there is only one stability region if $K > f(\omega)$. There is a possibility of multiple stability regions if $K < f(\omega)$. Our numerical plot, in Fig. 1(a), of the curves $\tau_1(n; K)$ and $\tau_2(n; K)$ reveals that the region between $\tau = 0$ and $\tau = \tau_1(0; K)$ is the only stability region possible for small values of ω . However as the value of ω is increased, the stability regions can be specified by $0 < \tau_0 < \tau_1(0; K)$, and $\tau_2(n; K) < \tau < \tau_1(n; K)$ where $n > 0$. In Fig. 1(b) the critical curves are plotted from Eqs. (10) and (11) for such a large value of ω , namely $\omega = 30$ and the multiple stability regions are represented by the shaded portions. It is interesting to note that a similar situation occurs in the case of two or more coupled limit cycle oscillators that are coupled by a time delayed linear coupling. This was investigated in detail in [21,22], where the collective stability regions were termed amplitude death regions or death islands in the K space.

We conclude this section by carrying out a stability analysis of the origin in the (τ, K) plane for a fixed value of ω . Using Eqs.(5-6) we write below the critical curves which are non intersecting.

$$K(\tau) = \frac{!}{\sin(\tau)}; \text{ and } a(\tau) = \frac{!}{\sin(\tau)} \cos(\tau); \quad (15)$$

We note that the above expressions for $K(\tau)$ and $a(\tau)$ have singularities at $\tau = n\pi$ and between any two successive singular points the expressions produce continuous curves in (τ, K) plane. Following Diekmann et al. [36], we define the following intervals where the sign

of the superscript of I indicates the sign of the function $\sin(\cdot)$ in that interval:

$$I_n = ((2n-1)-; 2n-); \quad I_n^+ = (2n-; (2n+1)-); \quad (16)$$

for $n = 0; 1; 2; \dots$. We restrict our attention, without loss of generality, to the case of $\omega = 0$. Hence we can define the following curves in $(a; K)$ plane.

$$C_n = f(a; K) = \left(\frac{(-!) \cos(\cdot)}{\sin(\cdot)}, \frac{(-!) \sin(\cdot)}{\sin(\cdot)} \right) \in 2 I_n g; \quad (17)$$

$$D_n = f(a; K) = \left(\frac{(+!) \cos(\cdot)}{\sin(\cdot)}, \frac{(+!) \sin(\cdot)}{\sin(\cdot)} \right) \in 2 I_n g \quad (18)$$

These curves are parameterized by ω . The curves are degenerate at $\omega = n = 0$. For $\omega = 2n = 0; 1; 2; \dots$, both the curves C_n and D_n merge and there is another curve in addition to the above, defined by

$$C_R = f(K; a) \in a = K g \quad (19)$$

with $\omega = 2n = 0$. Likewise for $\omega = (2n+1) = 0; 1; 2; \dots$ the corresponding additional curve is defined by

$$C_R = f(K; a) \in a = K g \quad (20)$$

with $\omega = (2n+1) = 0$. We are now only left with the task of finding out the number of the eigenvalues in the right half plane on either side of the curves C_n and D_n . For our particular problem it is possible carry out this analysis in an exact manner. Let $F(a; K; \omega) = a - i\omega + K e^{-i\omega t} = 0$ be the eigenvalue equation. Define $G_1 = \operatorname{Re} F$, $G_2 = \operatorname{Im} F$, and at $\omega = 0$ define a matrix M by,

$$M = \begin{matrix} \frac{\partial G_1}{\partial a} & \frac{\partial G_1}{\partial K} & \omega \\ \frac{\partial G_2}{\partial a} & \frac{\partial G_2}{\partial K} & \end{matrix} : \quad (21)$$

We now make use of proposition 2.13 (in Chapter XI) of Diekman et al [36] to determine the positions of the eigenvalues in the complex plane with respect to the curves $(a(\cdot); K(\cdot))$. The proposition states that the critical roots are in the right half-plane in the parameter region to the left of the curve $(a(\cdot); K(\cdot))$, when we follow this curve in the direction of increasing ω , whenever $\det M < 0$ and to the right when $\det M > 0$. In the present case, on both the curves C_n and D_n , the matrix is given by

$$M = \begin{matrix} 1 & \cos(\cdot) & \omega \\ 0 & \sin(\cdot) & \end{matrix} : \quad (22)$$

and hence $\det M = \sin(\cdot)$. It is easily seen that $\det M > 0$ on C_n^+ , D_n^+ , and $\det M < 0$ on C_n , D_n . And finally we know that the stability region for $\omega = 0$

is given by $a < K$. Combining these facts we present our results for the stability region and the number of eigenvalues in Fig. 2 for a typical set of parameters. The amplitude death region is the region where there are no (i.e. zero) eigenvalues in the right half plane.

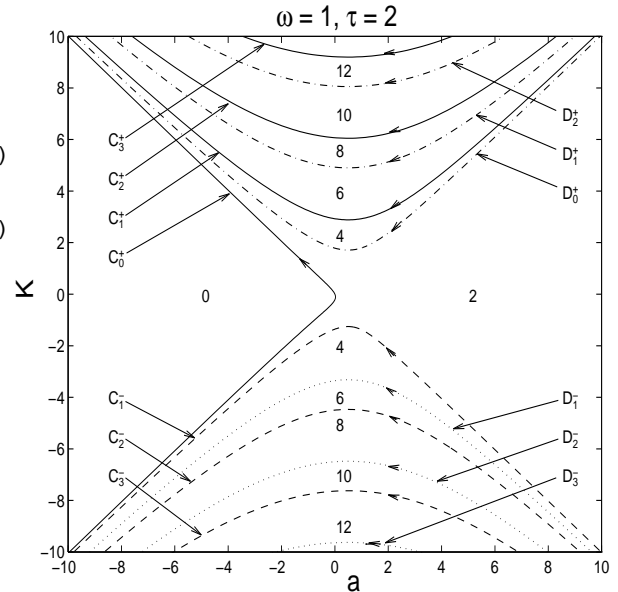


FIG. 2. Critical curves in (a, K) plane. The numbers indicate the number of eigenvalues in the right half plane of the complex eigenvalue space. The amplitude death region is the region where there are zero eigenvalues in the right half plane. The arrow on each curve shows the direction along which increases.

B. Periodic Solutions

We now examine the region where the origin is unstable. For $\omega = 0$ this region sustains periodic solutions as discussed in the introductory remarks of this section. We now look for periodic solutions in the presence of the time delay. For this, it is convenient to cast Eq. (3) in polar form. For simplicity, we also set $a = 1$. This implies that the oscillator without any kind of feedback has a unit circle as its periodic solution and the phase increases linearly on the circle. Writing Eq. (3) in polar coordinates we have,

$$r = (1 - r^2)r \quad K r(t) \cos(\omega t - \phi) \quad ; \quad (23)$$

$$\phi = -\omega \frac{r(t)}{r} \quad \sin(\omega t - \phi) \quad ; \quad (24)$$

where in the above the variables r and ϕ appearing with no arguments are the instantaneous values at time t . When the delay parameter $\tau = 0$, Eq. (3) has the time asymptotic periodic solution $Z(t) = \frac{1}{1-K} e^{i\omega t}$. For $\tau \neq 0$ let us assume a periodic solution of the form $Z(t) = R e^{i\omega t}$. That is we are looking for solutions of the form $r(t) = R$ and $\phi(t) = \omega t$, where R and ω are real constants.

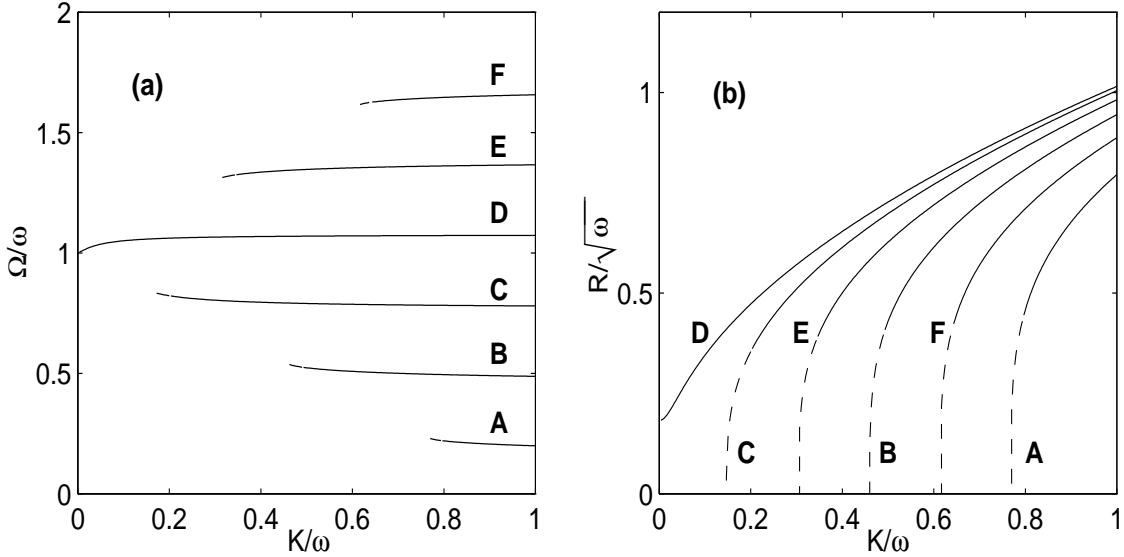


FIG . 3. Finite time delay leads to the existence of multiple periodic states, which can coexist with the primary limit cycle state. The frequencies and amplitudes of these states (for $\tau = 0.68$) are plotted as a function of the coupling strength K in (a) and (b) respectively. As the value of the strength of the feedback, K , is increased, the number of periodic orbits increases. In both the plots the dashed portions of the curves are unstable regions.

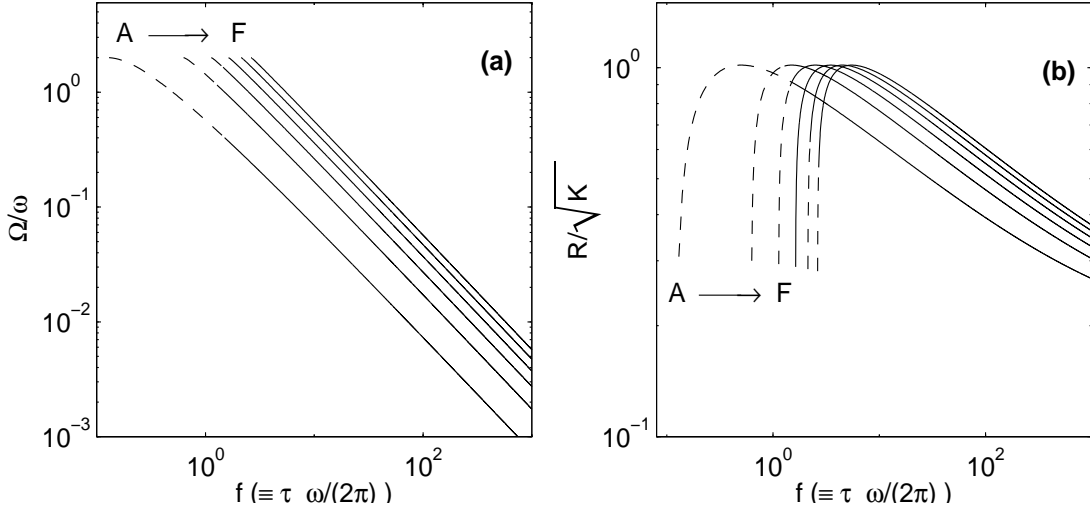


FIG . 4. The frequencies and amplitudes of the multiple periodic states are plotted as a function of $f = \tau \omega/(2\pi)$ in (a) and (b) respectively at $K = \tau = 30$. At large values of f , the frequency suppression is algebraic and is proportional to $1/f$. In both the plots the unstable portions are indicated by dashed lines.

In fact, it can be checked that this is the only solution which has a linear growth of the phase. Substituting this form in Eqs. (23) and (24) and after some algebra, we obtain the following relations for the amplitude and the frequency of the oscillator:

$$R = \frac{p}{1 - K \cos(\phi)}; \quad (25)$$

$$= \tau + K \sin(\phi) \quad (26)$$

Let $\phi = f/2 = \tau$ and thus $\phi = 2f$. From Eq.

(25) we see that the oscillator can now lie outside the unit circle when $\cos(\phi) < 0$, i.e. for the values of $\phi = (2n + \frac{1}{2})\pi$; $(2n + \frac{3}{2})\pi$ the amplitude of the limit cycle can increase beyond unity. However the amplitude is bounded for any value of ϕ since from (25), $\max(R) = \frac{p}{1 + K}$. So for any given K , the amplitude of the limit cycle stays in the interval $[\frac{p}{1 + K}; \frac{p}{1 + K}]$ for arbitrary values of ϕ . The above condition on ϕ can be used in Eq. (26) to infer bounds on the frequency of the limit cycle: $\tau - K \leq \omega \leq \tau + K$. Eq.

(26) adm its multiple solutions for the frequency ω . The L.H.S., $y_1 = \dots$, of (26) is a straight line and the R.H.S., $y_2 = ! + K \sin(2\omega t)$, is a sinusoidal curve with amplitude K and a shift of $!$ above the horizontal axis, $y = 0$. The multiple solutions (frequencies) are given by the intersection of the curves y_1 and y_2 . As the value of K is increased for a fixed value of $!$, the curve y_2 makes more and more intersections with y_1 and thus a set of multiple frequencies comes into existence. Similarly a variation in $!$ will also bring about changes in the number of possible solutions. But for all values of $!$, including for $! = 0$, multiple frequency solutions are a possibility. The existence of multiple frequencies is a characteristic feature of time delay systems and has been noted before in the context of the Kuramoto model with time delay [18] and in other studies [17, 21, 23]. It is interesting to observe that this basic feature is retained even for a single oscillator in the presence of time delayed feedback. These multiple frequency states that coexist with the lowest frequency state can be accessed by a suitable choice of initial conditions and have potential applications in coupled oscillator models of the human brain. In Fig. 3(a) we plot these multiple frequencies, ω , for $! = 30$ and $f = 3.25$. Fig. 3(b) shows the corresponding amplitudes of the multiple states. Whenever the time delay is equal to integer multiples of the intrinsic period of the oscillator (i.e. when f is an integer), some of these states merge. This can be inferred from the intersections of the amplitude curves in Fig. 3(b). At these points, the oscillator has two frequencies with a single amplitude. To find out these frequencies, let ω_1 and ω_2 be the two frequencies at these degenerate points. Substituting these values in the expression for R in (25), we get $\frac{1}{\omega_1^2} = \frac{1}{\omega_2^2} + \frac{m}{f}$, where m is an integer. As the delay parameter is increased, the frequency of the oscillation gets reduced. This is true for all the multiple frequency states that the system possesses. In Fig. 4(a) the normalized frequency of each of the states is plotted against the time delay on a log scale. The frequencies are suppressed at a rate proportional to the inverse of the time delay. Fig. 4(b) shows the corresponding amplitudes plotted against time delay. This feature of frequency suppression has been observed in the past for large coupled systems [18] and once again seems to have its roots in the behavior of a single oscillator in the presence of a time delayed feedback drive.

C. Stability of the Multiple States

The stability of the multiple periodic solutions can be obtained by linearizing about each of the solutions. The linearized matrix is given by

$$M_1 = \begin{pmatrix} A & B e^{-\omega t} & R C (1 - e^{-\omega t}) \\ \frac{C}{R} (1 - e^{-\omega t}) & B (1 - e^{-\omega t}) & \end{pmatrix};$$

where $A = 1 - 3R^2$; $B = K \cos(\omega t)$; and $C = K \sin(\omega t)$. The eigenvalue equation is given by $\det(M_1 - I) = 0$. In

the limit $\omega \rightarrow 0$ this yields $R = \frac{P}{1 - K}$, $A = 1 - 3(1 - K)$, $B = K$, and $C = 0$, so that $\omega = f_0 = 2(1 - K)g$. We thus recover the result that the periodic solution is stable for $\omega < 0$ when $K < 1$. For $\omega \neq 0$ we need to solve the eigenvalue equation numerically for which the following form is more convenient:

$$A_1 e^{2\omega t} + A_2 e^{\omega t} + A_3 + e^{-\omega t} A_4 + A_5 e^{-2\omega t} = 0;$$

where $A_1 = B^2 + C^2$, $A_2 = AB + B^2 - 2C^2$, $A_3 = AB + C^2$, $A_4 = A + B$ and $A_5 = 2B$. Our numerical results for the stability of the multiple periodic states are incorporated in Fig. 3 and Fig. 4 where the dashed portions of the curves indicate unstable regions.

III. NONLINEAR FEEDBACK EFFECTS

In this section we include the nonlinear feedback term ($K_2 \neq 0$) and examine the dynamics of the limit cycle oscillator in the presence of the complete feedback term f as given in (2). We then have,

$$Z(t) = (a + i! - jZ(t)^2)Z(t) \\ K_1 Z(t) - K_2 Z^2(t); \quad (27)$$

In order to distinguish the additional effects arising from the nonlinear feedback term we first turn off the time delay and examine the dynamics for $\omega = 0$. The fixed points of the system are found by setting the time derivative of Z to zero. In contrast to the earlier case of a linear feedback drive, there are now three fixed points of the system including the origin. In Table 1, we list the fixed points and expressions for the eigenvalues of linear perturbations around these fixed points,

TABLE I.

Symbol	index i	Fixed point (X_i ; Y_i)	Eigenvalues
D	0	(0; 0)	K_1 $-i!$
FP ₁	1	($\frac{K_2}{2} + \frac{p}{G}; \frac{1}{K_2}$)	K_1 T_1
FP ₂	2	($\frac{K_2}{2} - \frac{p}{G}; \frac{1}{K_2}$)	K_1 T_2

where $G = (\frac{K_2}{2})^2 - K_1^2 - \frac{!^2}{K_2^2}$, $K_1 = K_1 - a$ and $T_i = \sqrt{X_i^2 + Y_i^2} - !$. As we can see, the origin exists as a fixed point for all the values of the parameters a ; K_1 ; K_2 and $!$. However, it is stable only when $K_1 > 0$, i.e. when $K_1 > a$. The other two fixed points FP_1 and FP_2 exist in the region $G > 0$. This condition gives the curves $K_2 > (K_1)$ and $K_2 < (K_1)$, where $(K_1) = \frac{p}{2} - K_1 + \frac{K_1^2 + !^2}{2}$. This region overlaps with $K_1 > 0$. The bifurcation diagram is shown in Fig. 5. The regions marked by D, FP_1 and FP_2 are the regions in which the corresponding fixed points are

stable. The region D is bounded on the right hand side by $K_1 = a$. The region FP_1 is bounded by the curves

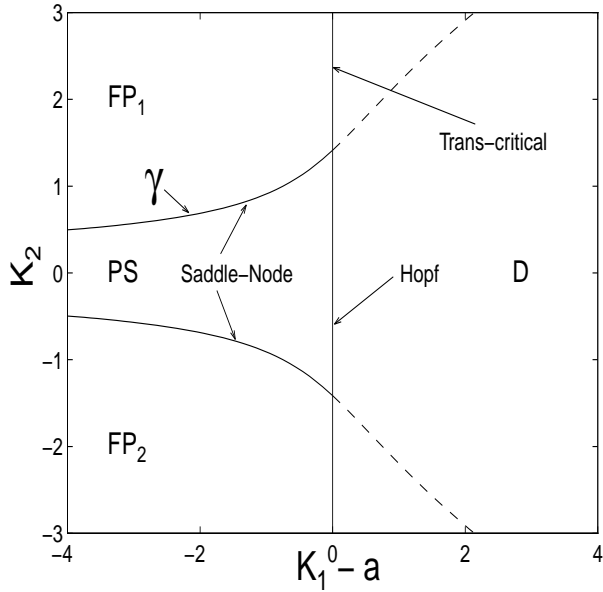


FIG. 5. The bifurcation diagram of Eq. (27) for $\gamma = 0$ in $(K_1; K_2)$ plane for $a = 1$, $\beta = 1$. D is the region of amplitude death, FP_1 and FP_2 are the regions of stability of the fixed points FP_1 and FP_2 respectively. The periodic solution is stable in the region PS .

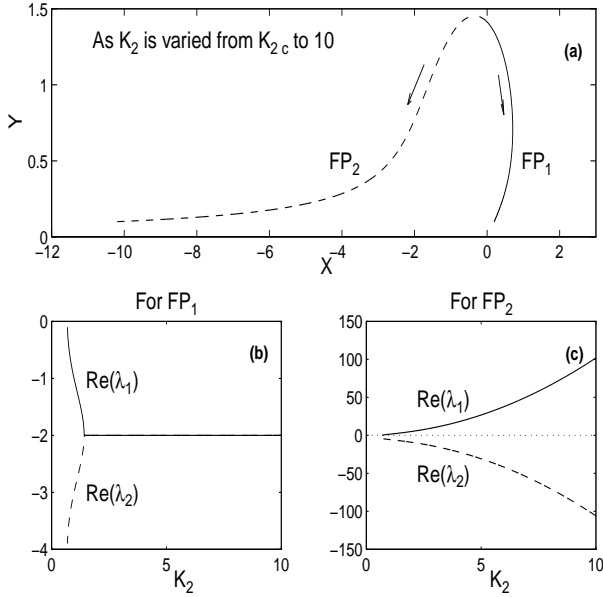


FIG. 6. The movement of the fixed points of Eq. (27) for $\gamma = 0$ ($a = 1$, $\beta = 1$, $K_1 = 1$) is shown in (a) as K_2 is varied from the critical value $K_{2c} = 0.6871$ to 10. The behavior of the real parts of the eigenvalues for the corresponding fixed points are plotted in (b) and (c) respectively and show that FP_1 is stable and FP_2 is unstable in this case.

$K_1 = 0$ and $K_2 = (K_1)$. The region FP_2 is bounded by

the curves $K_1 = 0$ and $K_2 = (K_1)$. The periodic solution is stable in the region $(K_1) < K_2 < (K_1)$ and $K_2 < K_1$. The movement of the fixed points in parameter space and the corresponding eigenvalues are shown in Fig. 6. Finally in Fig. 7 we draw the periodic orbit and the time evolution of the components of the limit cycle for a typical set of K_2 values. We now discuss some of the interesting features of this bifurcation diagram.

(i) Saddle-Node bifurcation. The periodic orbit develops a saddle at (FP_2) and a node at (FP_1) as K_2 is increased above (K_1) . Similarly as K_2 is decreased below (K_1) a node at (FP_2) and a saddle at (FP_1) are born. The periodic orbit is a circle for $K_2 = 0$ and the oscillator moves linearly on the circle with a frequency ω . As K_2 is increased or decreased the period of the limit cycle increases and tends to infinity on the curve $K_2 = (K_1)$. It is interesting to note that such a phenomenon of the period of synchronized oscillations tending to infinity and giving rise to a saddle-node pair has been observed experimentally by Crowley and Epstein [37] in Belousov-Zhabotinskii reactions. In our model for a driven single oscillator such a behavior arises from the presence of the simple quadratic nonlinear term. In Fig. 8 we plot the period of the limit cycle in the region PS as K_2 is increased keeping K_1 and β fixed.

(ii) Phase slips.

When the nonlinear feedback is absent, i.e. when $K_2 = 0$, the limit cycle is a circle and the phase of the oscillator increases linearly on the circle for all values of K_1 and

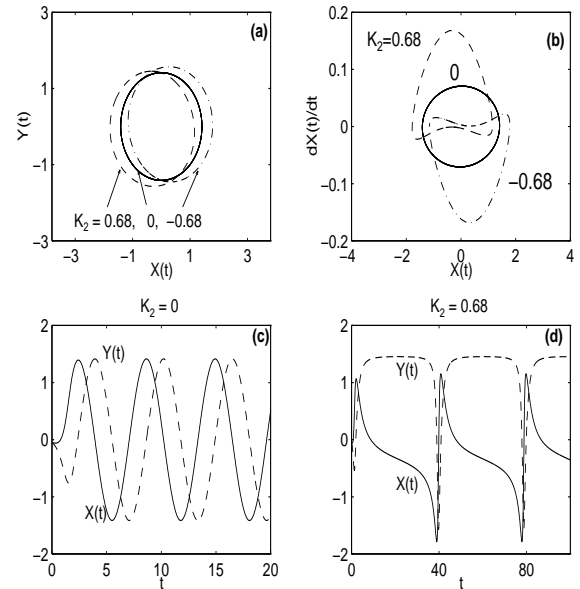


FIG. 7. The nature of the periodic orbits in the (a) X - Y space and in the (b) X - dX/dt space for $K_2 = 0.68; 0; -0.68$. The time evolutions of the individual amplitudes X and Y of the limit cycle oscillator are plotted in (c) for $K_2 = 0$ and in (d) for $K_2 = 0.68$ respectively. These orbits correspond to the region PS of Fig. 5.

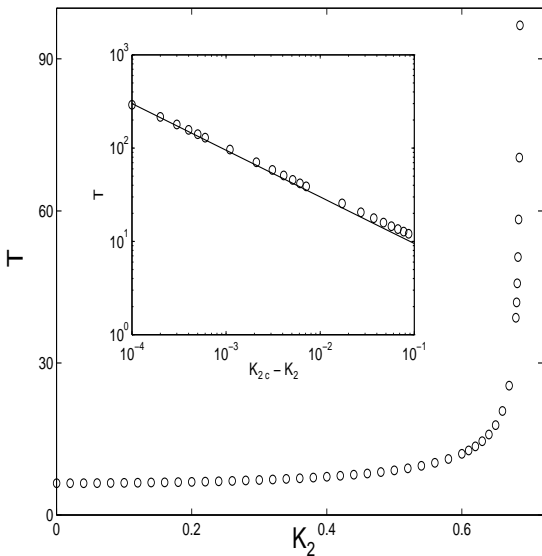


FIG. 8. The variation of the period of the limit cycle in the region P S of Fig. 5. as a function of K_2 for a fixed value of $K_1 = 1$. As K_2 is increased from 0 to (K_1) the period increases from $2 = 1$ to infinity with a scaling proportional to $1 = (K_{2c} - K_2)$ and leading to a saddle-node bifurcation. The inset shows the scaling. The solid curve is a plot of $T = K_{2c} - K_2$.

in the region where the origin is unstable. As the magnitude of K_2 is increased from 0 to (K_1) the evolution of the phase of the oscillator on the circle takes on a non-linear character. It begins to spend more time at certain values of the phase and less and less time at other values. Close to the curves (K_1) the oscillator shows clear phase slips as seen in Fig. 9. The oscillator spends most of the time in the smallest range of the phase and suffers a slip of 2π at regular intervals with a period T as shown in Fig. 8. This phase slip ends with phase quenching on the boundary of (K_1) . In this state the phase of the oscillator is a constant and such a state is often referred to as phase death. The phenomenon of phase slips plays an important role in the process of transition towards a synchronized state in a system of a large number of coupled limit cycle oscillators and has been the subject of some recent investigations [39].

From the above it is clear that our simple model of a single Hopf oscillator with a quadratic nonlinear feedback term is capable of displaying a rich variety of dynamics – many of which are normally found in higher dimensional systems of many coupled oscillators. The principal contribution of the quadratic nonlinear term is to introduce additional fixed points, whose stability properties give rise to interesting features in the dynamics of the oscillator. We now return to our full feedback model and include the effect of finite time delay on the dynamical characteristics of the oscillator. Since we now have an infinite dimensional system, the phase space dynamics can in general be quite complicated and change significantly

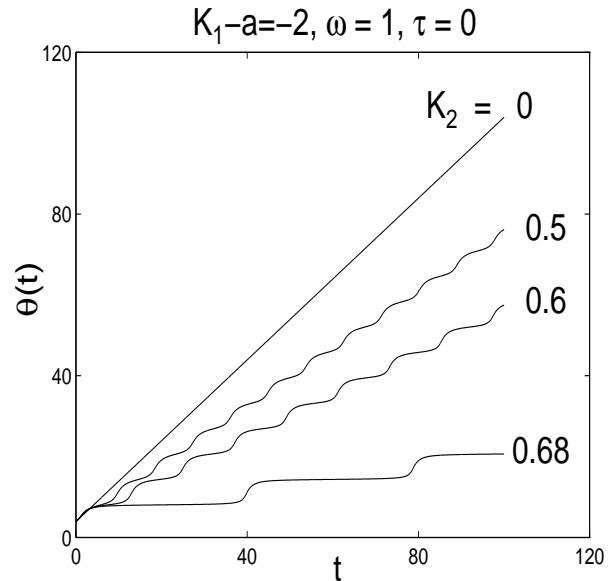


FIG. 9. Phase slips of the limit cycle oscillator for $\omega = 0$, $K_1 = 1$, $\beta = 1$, and $a = 1$. The phase of the limit cycle oscillator evolves linearly on the circle when there is no nonlinear feedback. With increasing K_2 one clearly sees the phase slips suffered by the oscillator.

as a function of the time delay parameter τ .

We proceed first to carry out a linear perturbation analysis around the three fixed points and then construct the bifurcation diagram for fixed values of τ through detailed numerical investigations. The analysis of the stability of the origin remains unchanged by the presence of the K_2 term since its contribution vanishes in the linear limit. So its behavior can be discerned from the previous section (e.g. see Fig. 1 (a) where we saw that the amplitude death region shrinks and moves to the right of the curve $K_1 = 0$ as τ is increased from 0 and vanishes at a certain critical value. Depending on the strength of β it may reappear again. For the present study we choose $\beta = 1$ and $\tau = 0.5$, which is much less than the intrinsic time period 2π . For this value the amplitude death region disappears and the origin is always unstable. The fixed points $F P_1$ and $F P_2$ are again the same as discussed in the previous section, but their stability properties are now significantly modified due to finite time delay effects.

Let $Z = (X + iY)$ be one of the non-zero fixed points of the system. A linearization about Z of (27) yields the following equation:

$$\begin{aligned} \underline{z}(t) = & (a + i\beta - 2\beta Z^{-1})z \\ & - Z^{-2}z - (K_1 + 2K_2Z^{-1})z(t-\tau); \end{aligned} \quad (28)$$

where $z = Z - \bar{Z}$ and \bar{z} is the complex conjugate of z . Write $z(t) = x(t) + iy(t)$ and assume each component to vary as $e^{\lambda t}$, where λ is the eigenvalue of the linearized matrix M_2 given by

$$M_2 = \begin{bmatrix} A & B e^{-\lambda\tau} & 2X^{-2} & 2K_2Y e^{-\lambda\tau} & C_1 \\ 2K_2Y e^{-\lambda\tau} & + C_2 & A & B e^{-\lambda\tau} & 2Y^{-2} \end{bmatrix} : \quad (29)$$

Here $A = a(X^2 + Y^2)$, $B = K_1 + 2K_2X$, $C_1 = 1 + 2XY$, and $C_2 = 1 - 2XY$. The eigenvalue equation is given by $\det(M_2 - I) = 0$, which can be written in the following way.

$$(A - Be - \tau)^2 - 2(X^2 + Y^2)(A - Be - \tau) + (2K_2Y - e - \tau)^2 = 0; \quad (30)$$

The evolution of τ in the complex plane as K_1 and K_2 are varied decides the stability of the fixed points. The relation between K_1 and K_2 for the critical boundary is not very transparent from the above equation. We use Eq. (30) to determine these boundaries numerically and present the bifurcation diagram in Fig. 10. The regions labelled FP_1 and FP_2 correspond to the stability regions of the corresponding fixed points respectively. When K_2 is small and one is in the region where the origin is unstable but FP_1 and FP_2 are stable, the limit cycle orbit preserves its identity and the results are similar to those discussed in earlier sections. As K_2 is increased in magnitude however interesting new orbits and features appear which we discuss below.

(i) The simple periodic orbit.

The simple periodic orbit (limit cycle) exists for all small values of K_2 in the region marked as P . This loses stability in a saddle-node bifurcation on boundaries of FP_1 and FP_2 , which appear as an 1-period limit cycle. However, for larger values of time delay, (for example $\tau = 1.0$)

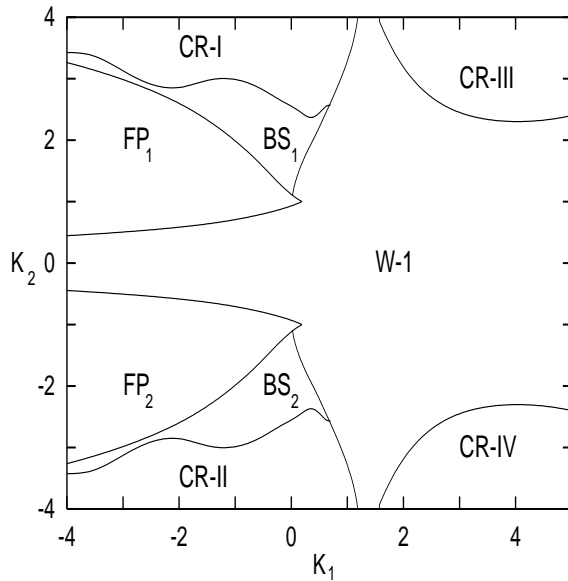


FIG. 10. Bifurcation diagram of Eq. (27) for $\tau = 0.5$, $a = 1$, and $1 = 1$. The areas marked FP_1 and FP_2 refer to stability domains of these fixed points, the region $W-1$ sustains limit cycle orbits encircling the origin (winding number 1), the regions BS_1 ; BS_2 contain combinations of phase reversing, radially trapped or spiraling solutions in a brythmic existence, and the regions marked $CR-I$; $CR-II$; $CR-III$; $CR-IV$ exhibit chaotic behavior interspersed with periodic windows.

as shown in Fig. 11), the bifurcation occurs with a finite time period limit cycle. This is one major difference in the bifurcation sequence of saddle-node in the presence of time delay.

(ii) Phase reversals.

The periodic orbit is a simple circle for small values of K_2 but as K_2 increases there are regions where the orbit acquires an additional loop as shown in Fig. 12 (a). This loop is not around the origin so that the winding number of the periodic orbit continues to be one. However the phase of the orbit as measured from the origin appears to undergo a reversal in that region (Fig. 12 (d)), in contrast with the phase slip behavior discussed earlier. Such periodic orbits for a single oscillator have been observed for externally driven systems and basically arise due to the excitation of higher harmonics from the resonant interaction of the external driver with the basic oscillator [40]. They cannot exist for a single autonomous oscillator in the absence of time delay due to dimensional constraints. However the presence of time delay in our autonomous model increases the dimensionality of the system and hence permits the existence of such orbits. This is a new kind of orbit which does not seem to have been noticed or discussed before in the context of large systems of coupled oscillators and it would be worthwhile looking for their existence in such systems.

(iii) Effect of time delay on phase slips.

The phenomenon of phase slips continues to exist for non zero values of time delay as well. To study the effect of

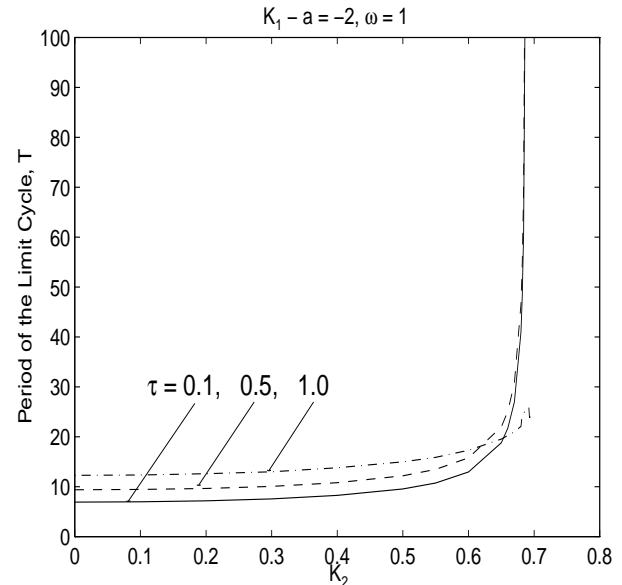


FIG. 11. Effect of time delay on the period of the limit cycle oscillator. For shorter time delays the period of the limit cycle becomes infinite at a critical value of K_2 and disappears in a saddle-node bifurcation. For longer time delays the period remains finite at the critical value of bifurcation. $K_1 = -1$, $a = 1$, and $1 = 1$.

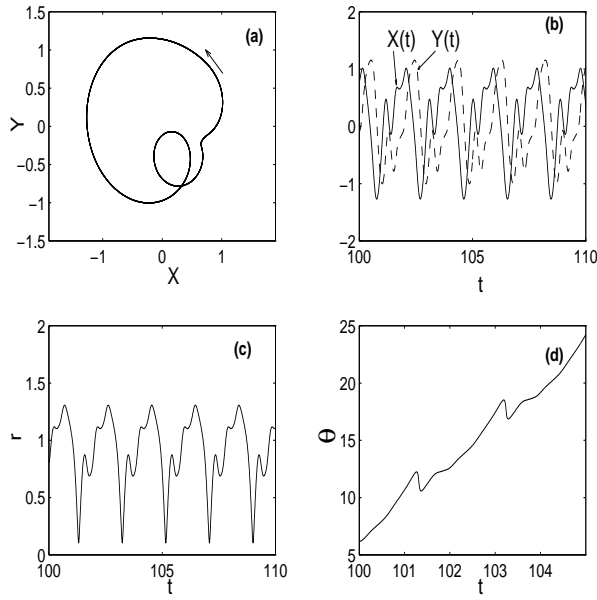


FIG. 12. A phase reversing orbit. The orbit of the limit cycle in the (a) X – Y space, (b) the temporal evolution of the individual components X and Y , (c) the temporal evolution of the absolute amplitude $r = \sqrt{X^2 + Y^2}$ and (d) the temporal evolution of the phase as measured from the origin are plotted for $K_2 = 4.0$; $K_1 = 1.4$; $a = 1$; $\beta = 1$, and $\omega = 0.5$.

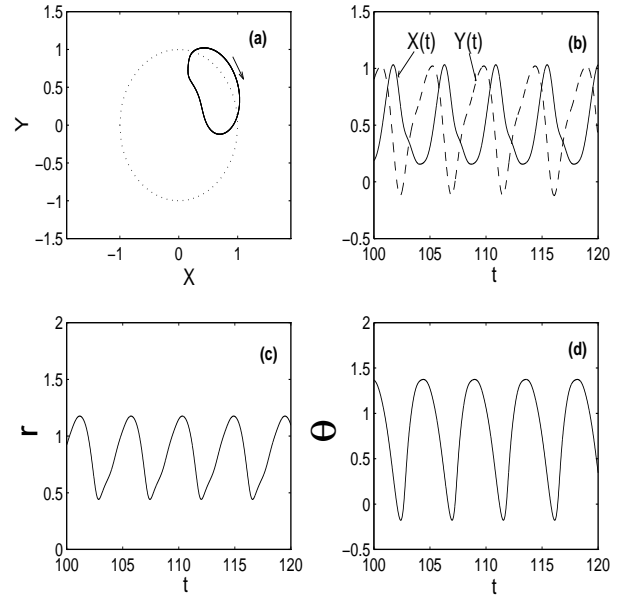


FIG. 14. A radially trapped orbit. The orbit of the limit cycle in the (a) X – Y space, (b) the temporal evolution of the individual components X and Y , (c) the temporal evolution of the absolute amplitude $r = \sqrt{X^2 + Y^2}$ and (d) the temporal evolution of the phase as measured from the origin are plotted for $K_2 = 1.9$, $K_1 = 0.6$, $a = 1$, $\beta = 1$, and $\omega = 0.5$. The radially trapped orbit is a periodic orbit around one of the unstable nonzero fixed points (in this case F_P_1).

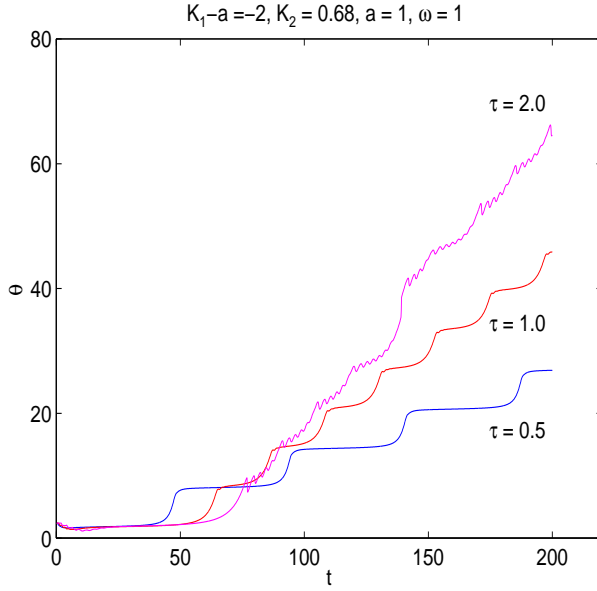


FIG. 13. Effect of time delay on the phase slips. Time delay smoothens the phase slips. ($K_1 = 1$; $a = 1$; $\beta = 1$, and $K_2 = 0.68$.)

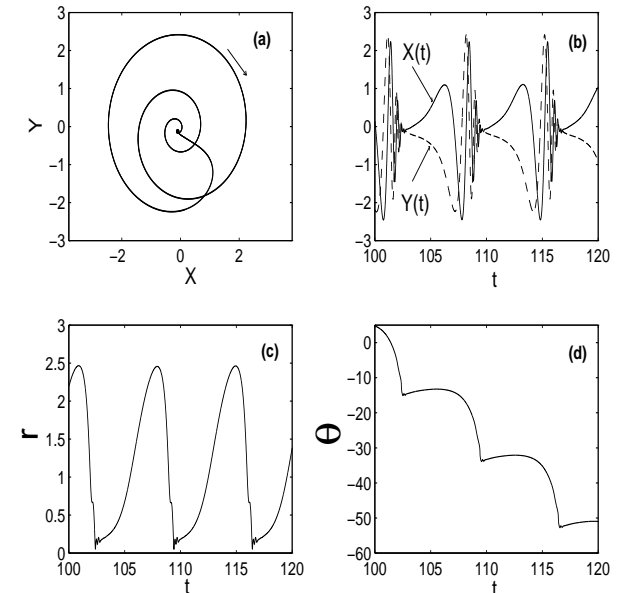


FIG. 15. A spiraling orbit. The orbit of the limit cycle in the (a) X – Y space, (b) the temporal evolution of the individual components X and Y , (c) the temporal evolution of the absolute amplitude $r = \sqrt{X^2 + Y^2}$ and (d) the temporal evolution of the phase as measured from the origin are plotted for $K_2 = 3$; $K_1 = 0.2$; $a = 1$; $\beta = 1$, and $\omega = 0.5$.

time delay on the phase slips, we examine Fig. 9 and choose the parametric values corresponding to the phase slips shown by the bottom most curve, i.e. for $K_2 = 0.68$, and introduce finite time delay. The results are shown in Fig. 13. Time delay has the effect of reducing the sharpness of the phase slips and, at the same time, increasing the angular speed as seen by the slope of $\dot{\theta}$. For longer time delays, (e.g. for $\tau = 2.0$ in the figure), phase slips are less evident and in fact the orbits exhibit chaos.

(iv) Radially Trapped Solutions.

In addition to the phase reversing solutions, we also observe one more kind of orbit in the region where F_{P_1} or F_{P_2} loses stability. These are orbits that simply encircle the unstable fixed point (F_{P_1} or F_{P_2}) and have winding number zero around the origin. We call them radially trapped solutions because, viewed from the origin, they are restricted to a region of phase space and seem to oscillate within a restricted physical space. One such radially trapped orbit is shown in Fig. 14. The oscillator moves clockwise.

(v) Spiraling solutions.

Another interesting periodic orbit that we find is shown in Fig. 15(a) and can best be described as a spiraling orbit since the amplitude of the limit cycle (in the

$(X;Y)$ space) first spirals out and then comes back to its original state. The phase changes have a step like character. Such orbits exist in a thin region near the radially trapped solutions.

(vi) Bhythymicity.

The phase reversing and the radially trapped solutions are found to coexist in the same parameter regime (e.g. $K_2 = 1.6$, $K_1 = 0.2$, $a = 1$, $\beta = 1$, $\gamma = 0.5$ as shown in Fig. 16(a)) and thus exhibit a birhythymic behavior. In fact, birhythymicity appears to occur also for the spiraling and trapped solutions and is spread out over a large region of the parameter space. These are marked as B_{S_1} and B_{S_2} in Fig. 10. Birhythymicity is a common phenomenon in many biological models, and is currently the subject of many studies [38]. The switching between the two states can take place by the slightest perturbation to the initial states $(X(0);Y(0))$. A plot of the basins of attraction for the two states of Fig. 16(a) is shown in Fig. 16(b) in the space of the initial conditions $(X(0);Y(0))$. The dotted region is the basin of attraction for the phase reversing solution and the white region is that for the radially trapped solution. To generate this figure the initial conditions chosen were $X(0) = X(t=0) + 2[\cdot;0]$, and $Y(0) = Y(t=0) + 2[\cdot;0]$.

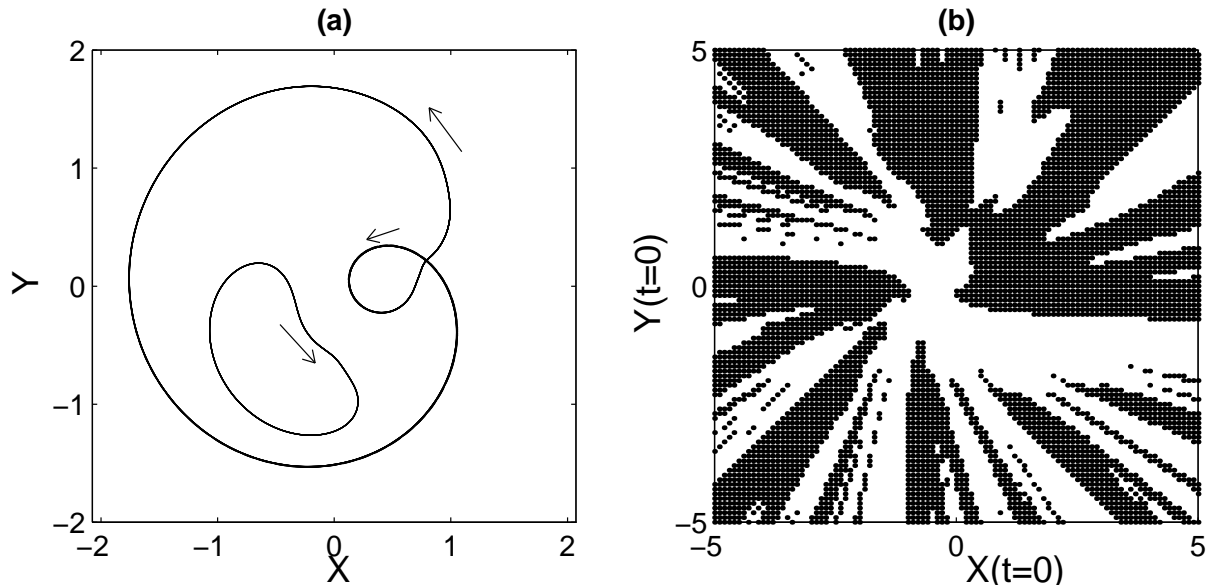


FIG. 16. Bhythymicity. (a) Radially trapped and the phase reversal solution coexisting for $K_2 = 1.6$, $K_1 = 0.2$, $a = 1$, $\beta = 1$, and $\gamma = 0.5$. (b) A plot of the basins of attraction for these two states in the space of the initial conditions $(X(0);Y(0))$. The dotted region is the basin of attraction for the phase reversing solution and the white region is that for the radially trapped solution. To generate this figure the initial conditions chosen were $X(0) = X(t=0) + 2[\cdot;0]$, and $Y(0) = Y(t=0) + 2[\cdot;0]$.

(vii) Routes to Chaos.

Our nonlinear model equation (27) also exhibits regions of temporal chaos and we have investigated this phenomenon in some detail, particularly with regard to

routes to chaos. The route to chaos appears to be a strong function of the parameters $K_1; K_2$ and γ and the type of periodic orbit existing in a particular parameter domain. We find evidence of several distinct routes to

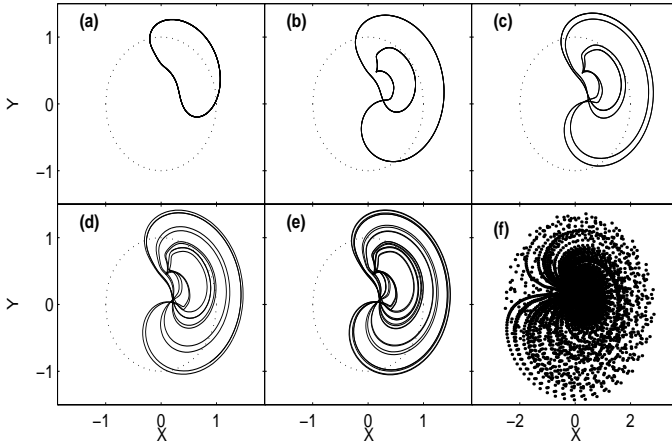


FIG. 17. The radially trapped orbit of the limit cycle can undergo a period doubling sequence to the chaotic state. Some of the periodic orbits with (a) Period-1, $K_2 = 1:6$, (b) Period-2, $K_2 = 2:1$, (c) Period-4, $K_2 = 2:13$, (d) Period-8, $K_2 = 2:18$, (e) Period-16, $K_2 = 2:186$, and (f) a chaotic orbit, $K_2 = 2:6$ are shown. The other constants are $K_1 = 0:2$, $a = 1$, $\beta = 1$, and $\gamma = 0:5$. The scale of (d) is twice that of the other plots.

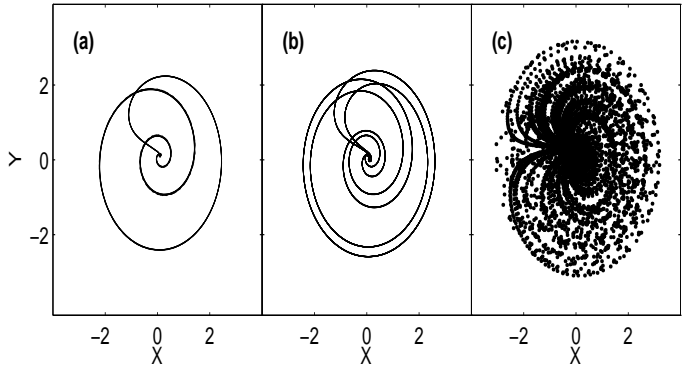


FIG. 19. The spiraling orbit period doubles once and then goes to a chaotic state as typically shown in the sequence, (a) $K_2 = 3:0$, (b) $K_2 = 3:121$, (c) $K_2 = 3:128$. The plot in (c) is generated with dots using a time record of length 80 intrinsic periods after leaving out 1273 periods of transients. The time step chosen for the integration is 0:004. The other constants are $K_1 = 0:2$, $a = 1$, $\beta = 1$, and $\gamma = 0:5$.

IV. SUMMARY AND DISCUSSION

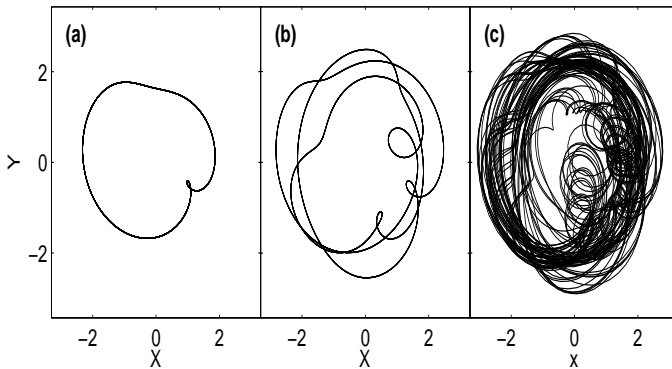


FIG. 18. The phase reversing orbit can bifurcate into a period-3 orbit leading to a chaotic attractor. These typical states are shown for (a) $K_2 = 2:2$, (b) $K_2 = 2:5$, (c) $K_2 = 2:712$. The other constants are $K_1 = 4:2$, $a = 1$, $\beta = 1$, and $\gamma = 0:5$.

chaos in our single model system. For example, the radially trapped solutions appear to follow the period doubling route to chaos as shown in the sequence of plots in Fig. 17. The phase reversing solutions appear to go to the chaotic state in several different ways. The limit cycle can make a transition from a simple orbit to a quasi-periodic state. Or a period 1 state can make a transition to a period-3 orbit. Such a transition is shown in Fig. 18. We find a large window of Period-3 orbits starting from $K_2 = 2:283$ for the parameters given in Fig. 18. The spiraling orbits appear to undergo a single period doubling bifurcation and then a sudden transition to chaos. An example is shown in Fig. 19. Finally, in Fig. 20, we display the detailed bifurcation diagrams (obtained from Poincaré section plots) corresponding to these scenarios.

We have studied the dynamics of a single Hopf bifurcation oscillator in the presence of an autonomous time delayed feedback. The feedback term has both a linear component and a simple quadratic nonlinear term. Using a combination of analytic methods and numerical analysis, we have investigated the temporal dynamics of this system in various regimes characterised by the natural parameters of the oscillator (e.g. its frequency ω , linear growth rate a), strengths of the feedback components (K_1, K_2) and the time delay parameter, τ . Our principle results are presented in the form of bifurcation diagrams in these parameter spaces. These reveal a rich variety of temporal behavior including time delay induced stabilisation of the origin, multiple frequency states, frequency suppression, phase slips, saddle node bifurcations, and chaotic behavior. In addition, some of the periodic orbits exhibit novel behavior such as phase reversals, radial trapping, spiraling oscillations in amplitude space, and brythymicity, which can be understood in terms of the stability of the fixed points and the nature of the feedback terms. One of the attractive features of these results is that many of them have been observed in the collective behavior of larger systems such as the Kuramoto model or the generalised Kuramoto model. This has been one of our major motivations for constructing this model – as a sort of paradigm to obtain and investigate these states in a simple manner. The feedback term not only model the collective drive that a single oscillator feels in a larger system, but also incorporate time delay in an autonomous manner. Time delay frees the dimensional constraints of the system (the system is essentially 1-dimensional) and this might be the reason why its temporal dynamics resembles so much that of larger dimensional systems.

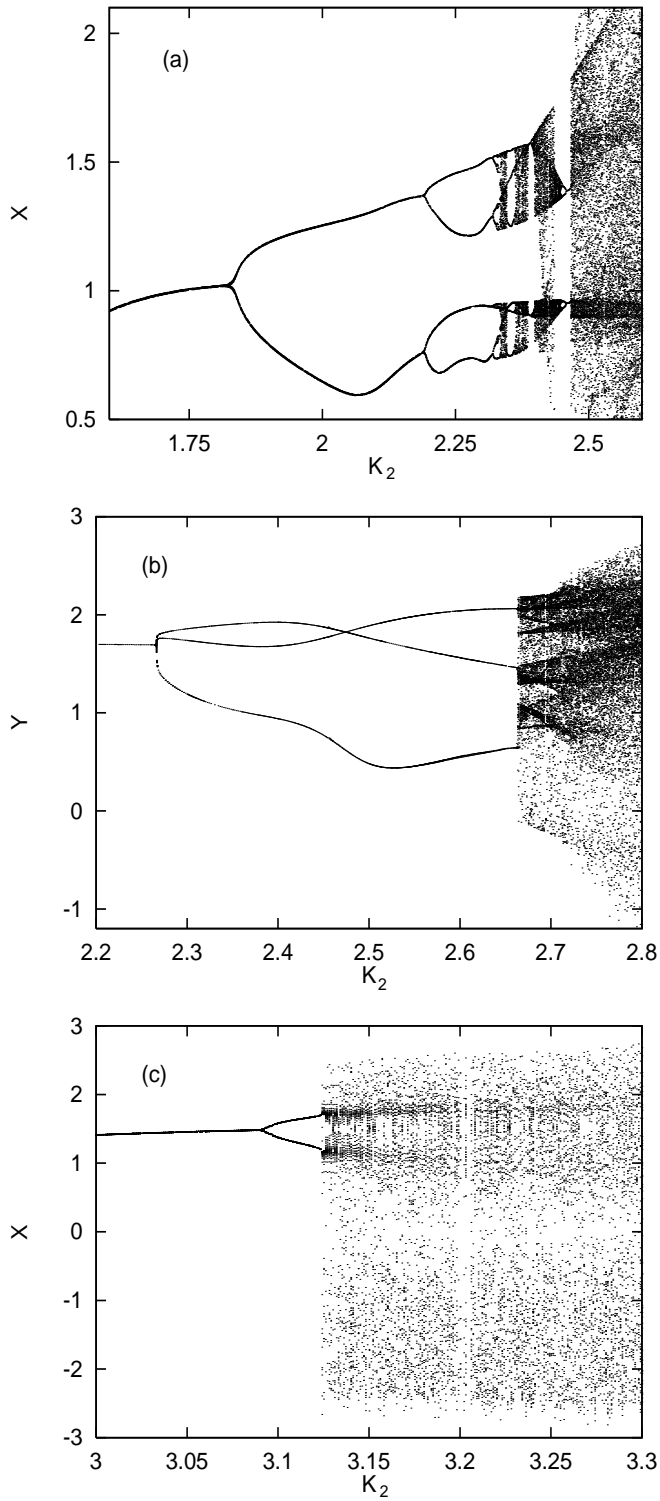


FIG. 20. Typical bifurcation diagrams generated by Poincaré section techniques showing (a) phase trapped, (b) phase reversing, and (c) spiraling solutions. The plots show the value of (a) X in the plane $Y = 0$, $Y < 0$, $K_1 = 0.25$, (b) Y in the plane $X = 1.4$, $X < 0$, $K_1 = 4.3$ and (c) X in the plane $Y = 2$, $Y < 0$, $K_1 = 0.2$. The other constants are $a = 1$; $\beta = 1$; and $\gamma = 0.5$.

Our results may therefore be useful for gaining better insights into the behavior of such large systems. As an example, the large window of $W = 3$ orbits of our model appears to have a correspondence to the transition region between the incoherent and chaotic states of the generalised Kuramoto model. We have found that the oscillators in the wings of the frequency distribution of a large collection of oscillators in the mean field model begin to acquire the $W = 3$ temporal states in that region and play an important role in the transition mechanism [41]. A detailed understanding of their dynamical behavior can thus help us in addressing some of the outstanding problems in this area, such as the nature of transition between low dimensional chaos and turbulence. Our model can also find more direct applications in simulation studies for feedback control of individual physical, chemical or biological entities that have the basic nonlinear characteristics of our Hopf oscillator, such as in single mode semiconductor lasers, relativistic magnetrons, chemical oscillations, biological rhythms in single nerve cells, etc. In fact, our basic Hopf oscillator model (without the feedback term) is mathematically related to the well known van der Pol oscillator equation, which displays relaxation oscillations. Retaining the quadratic nonlinearity (the Z^2 term) introduces a nonlinear Mathieu equation term in the van der Pol oscillator equation. The resultant nonlinear equation can physically represent parametric excitation of relaxation oscillations and can be used to model a number of physical or biological systems. It may be possible in such simple systems to then seek experimental verification of some of the novel temporal states displayed by our model.

^y E-mail: tapovan@plasma.ernet.in
^z E-mail: abhijit@plasma.ernet.in

- [1] M. K. M. C. Linton, Menstrual Synchrony and Suppression, *Nature* 229 (1971) 244.
- [2] P. DeNeef, H. Lashinsky, Van der Pol model for unstable waves on a beam plasma system, *Phys. Rev. Lett.* 31 (1973) 1039.
- [3] A. T. Winfree, *The Geometry of Biological Time*, Springer-Verlag, New York, 1980.
- [4] A. T. Winfree, *The Three-Dimensional Dynamics of Electrochemical Waves and Cardiac Arrhythmias*, Princeton University Press, Princeton, NJ, 1987.
- [5] Y. Kuramoto, I. Nishikawa, Statistical mechanics of large dynamical systems. Case of a phase transition in oscillator communities, *J. Stat. Phys.* 49 (1987) 569.
- [6] J. Benford, H. Sze, W. W. Sze, R. R. Smith, B. Harteneck, Phase Locking of Relativistic Magnetrons, *Phys. Rev. Lett.* 62 (1989) 969.
- [7] D. Golomb, D. Hansel, B. Shraiman, H. Sompolinsky, Clustering in globally coupled phase oscillators, *Phys.*

Rev. A 45 (1992) 3516.

[8] S. I. D'oum bouya, A. F. M unster, C. J. D oona, F. W . Schneider, Deterministic chaos in serially coupled chemical oscillators, *J. Phys. Chem.* 97 (1993) 1025.

[9] J. J. Collins, I. N. Stewart, Coupled Nonlinear Oscillators and the Symmetries of Animal Gaits, *J. Nonlinear Sci.* 3 (1993) 349.

[10] H. Daido, Onset of cooperative entrainment in limit-cycle oscillators with uniform all-to-all interactions: bifurcation of the order function, *Physica D* 91 (1996) 24, and references therein.

[11] L. M. Pecora, Synchronization conditions and desynchronizing patterns in coupled limit-cycle and chaotic systems, *Phys. Rev. E* 58 (1998) 347.

[12] K. Nakajima, Y. Sawada, Experimental studies on the weak coupling of oscillatory chemical reaction systems, *J. Chem. Phys.* 72 (1980) 2231.

[13] K. Bar-Eli, On the stability of coupled chemical oscillators, *Physica D* 14 (1985) 242.

[14] D. G. Aronson, G. B. Ermentrout, N. Kopell, Amplitude response of coupled oscillators, *Physica D* 41 (1990) 403.

[15] P. C. Matthews, S. H. Strogatz, Phase diagram for the collective behavior of limit cycle oscillators, *Phys. Rev. Lett.* 65 (1990) 1701.

[16] P. C. Matthews, R. E. Mirolo, S. H. Strogatz, Dynamics of a large system of coupled nonlinear oscillators, *Physica D* 52 (1991) 293, and references therein.

[17] H. G. Schuster, P. Wagner, Mutual entrainment of two limit cycle oscillators with time delayed coupling, *Prog. Theor. Phys.* 81 (1989) 939.

[18] E. N. Dierckx, H. G. Schuster, D. Kamban, Collective frequencies and metastability in networks of limit-cycle oscillators with time delay, *Phys. Rev. Lett.* 67 (1991) 2753.

[19] Y. Nakamura, F. Tomiaga, T. M. Nakata, Clustering behavior of time-delayed nearest-neighbor coupled oscillators, *Phys. Rev. E* 49 (1994) 4849.

[20] S. Kim, S. H. Park, C. S. Ryu, Multistability in coupled oscillator systems with time delay, *Phys. Rev. Lett.* 79 (1997) 2911.

[21] D. V. R. Reddy, A. Sen, G. L. Johnston, Time delay induced death in coupled limit cycle oscillators, *Phys. Rev. Lett.* 80 (1998) 5109.

[22] D. V. R. Reddy, A. Sen, G. L. Johnston, Time delay effects on coupled limit cycle oscillators at Hopf bifurcation, *Physica D* 129 (1999) 15.

[23] M. K. S. Yeung, S. H. Strogatz, Time delay in the Kuramoto model of coupled oscillators, *Phys. Rev. Lett.* 82 (1999) 648.

[24] P. C. Bressloff, S. Coombes, Travelling Waves in chains of pulse-coupled integrate-and-fire oscillators with distributed delays, *Physica D* 130 (1999) 232.

[25] W. K. Erigen, Kinetics of the Circulating-Fuel Nuclear Reactor, *J. Appl. Phys.* 25 (1954) 702.

[26] R. D. D'river, A Two-Body Problem of Classical Electrodynamics: the One-Dimensional Case, *Ann. Phys.* 21 (1963) 122.

[27] K. Miyakawa, K. Yamada, Entrainment in coupled saltwater oscillators, *Physica D* 127 (1999) 177.

[28] P. Tass, J. Kurths, M. G. Rosenblum, G. Guastini, H. Hefter, Delay-induced transitions in visually guided movements, *Phys. Rev. E* 54 (1996) R2224.

[29] A. D. Estexhe, Stability of periodic oscillations in a network of neurons with time delay, *Phys. Lett. A* 187 (1994) 309.

[30] J. M. Cushing, Periodic Solutions of Volterra's Population Equation with Hereditary Effects, *SIAM J. Appl. Math.* 31 (1976) 251.

[31] S. A. Campbell, J. Belair, T. O'hara, J. M.ilton, Complex dynamics and multistability in a delayed harmonic oscillator with delayed negative feedback, *Chaos* 5 (1995) 640.

[32] A. Fraikin, H. Lambard, Stochastic analysis of a Hopf bifurcation: Master equation approach, *J. Stat. Phys.* 41 (1985) 531.

[33] M. C. Mackey, A. Longtin, A. Lasota, Noise-induced global asymptotic stability, *J. Stat. Phys.* 60 (1990) 735.

[34] C. Kurmar, K. Schulten, Effect of noise and perturbations on limit cycle systems, *Physica D* 50 (1991) 311.

[35] K. Pyragas, Continuous control of chaos by self-controlling feedback, *Phys. Lett. A* 170 (1992) 421.

[36] O. Diekmann, S. A. van Gils, S. M. Verduyn Lunel, H.-O. Walther, *Delay Equations: Functional-, Complex-, and Nonlinear Analysis*, Springer-Verlag, New York, 1995.

[37] M. F. Crowley, I. R. Epstein, Experimental and theoretical Studies of a coupled chemical oscillator: phase death, multistability, and in-phase and out-of-phase entrainment, *J. Phys. Chem.* 93 (1989) 2496.

[38] A. Goldbeter, *Biological Oscillations and Cellular Rhythms*, Cambridge University Press, Cambridge, 1996.

[39] Z. Zheng, G. Hu, B. Hu, Phase Slips and Phase Synchronization of Coupled Oscillators, *Phys. Rev. Lett.* 81 (1998) 5318.

[40] S. Sato, M. Sano, Y. Sawada, Universal Scaling Property in Bifurcation Structure of Duffing's and of generalized Duffing's Equation, *Phys. Rev. A* 28 (1983) 1654.

[41] D. V. R. Reddy, A. Sen, G. L. Johnston, (to be published).